Ultrasonics 94 (2019) 102–108

Contents lists available at ScienceDirect

Ultrasonics

journal homepage: www.elsevier.com/locate/ultras

The nonlinear S_0 Lamb mode in a plate with a linearly-varying thickness

Zhongtao Hu[a,b], Zhiwu An[a,b,*], Yuanyuan Kong[a,b], Guoxuan Lian[a], Xiaomin Wang[a,b]

[a] State Key Laboratory of Acoustics, Institute of Acoustics, Chinese Academy of Sciences, Beijing 100190, China
[b] University of Chinese Academy of Sciences, Beijing 100049, China

ARTICLE INFO

Keywords:
Nonlinear Lamb wave
S_0 mode
Varying thickness plates

ABSTRACT

The aim of this paper is to investigate propagation characteristics and the generation mechanism of the nonlinear lowest-order symmetric Lamb mode (S_0) which propagates downslope in free elastic plates with slowly linearly varying-thickness. From theoretical analyses, in a low frequency-thickness product (*fd*) range, the S_0 mode is slightly dispersive, it is easy to generate, and it approximately satisfies the principle of the phase velocity matching. Therefore, if a S_0 mode is excited at a proper frequency in the low *fd* range, the amplitude of the second harmonic wave is linearly increasing in a certain propagating-distance, which is valuable for the practical NDE application of the second harmonic wave. Moreover, numerical simulations and experiments have been carried out to validate theoretical results. Our investigation of properties of the second harmonic wave can be applied to characterize and evaluate micro-structural damages in varying-thickness waveguides.

1. Introduction

Lamb waves are able to propagate long distances in waveguides. Combined with the highly sensitive nonlinear ultrasonic techniques [1–9], the nonlinear Lamb wave testing technique has been applied in many fields such as the fatigue damage assessment [10–12], the micro-crack detection [13–15], the thermal stress measurement [16–18], and the long bone evaluation [19]. At present, literatures about nonlinear Lamb waves mainly focused on uniform-thickness plates and shells. Notably, for a uniform-thickness plate, Zuo [7] and Wan [20] analyzed the nonlinear Lamb waves generated by the S_0 mode which is slightly dispersive and easy to generate in the low-frequency range. They proved that the S_0 mode could produce a significant second harmonic wave which increases linearly over a reasonable propagating-distance.

However, in practical applications, many plates have variable thicknesses [21–24]. We explored properties of the second harmonic wave, which is generated by the S_0 Lamb mode in a plate whose thickness varies linearly at a slow rate, in order to generate a highly-sensitive nonlinear Lamb wave. It is worth mentioning that the S_0 mode in this waveguide is approximately defined. In literatures [23–25], the low-order Lamb modes such as S_0, A_0, S_1, A_1, S_2 in varying thickness waveguides are supposed to be adiabatic, when these modes are slightly dispersive and the slope of the varying-thickness waveguide is less than 1°. In this paper, we studied the slight-dispersion S_0 mode propagating in a slowly varying-thickness plate (the slope is less than 1°), which can be treated as adiabatic. An adiabatic mode adapts to the thickness variation of the plate. That is, it locally corresponds to a guided mode of a plate with a uniform-thickness, and its phase velocity displays a smooth change in propagation, depending on the local thickness. Hence, a varying thickness plate can be considered as a series of plates with locally uniform-thicknesses, and the second harmonic wave in the plate can be solved by combining the solutions of the uniform-thickness plates of all the local thicknesses. Besides, for the adiabatic propagation of a S_0 mode, the energy flux of the incident wave can pass through the waveguide with almost no-reflection, and the mode-conversion effect is almost negligible for estimating the penetration energy of the incident wave [21,23,24,26].

2. Theoretical analyses

Nonlinear S_0 Lamb modes in a low *fd* range satisfies two conditions, that are an non-zero power flux and an approximate phase velocity matching [20]. The schematic of a varying- thickness plate is presented in Fig. 1. The waveguide is considered to be asymmetric with respect to the horizontal axis, and the proposed method in the following can be easily extended to the case of the symmetric geometry. Phase velocity dispersion curves for Lamb modes in aluminum plates with respect to *fd*, obtained by the bisection technique, is presented in Fig. 2[27]. When the selected S_0 Lamb mode at a given frequency propagates downslope in the plate, the decrease in thickness leads to a reduction in the wavenumber, and an increase in the phase velocity. That is, the black dot in Fig. 2 moves from the right to the left along the phase

* Corresponding author.
E-mail address: anzhiwu@mail.ioa.ac.cn (Z. An).

https://doi.org/10.1016/j.ultras.2018.11.013
Received 26 May 2018; Received in revised form 20 November 2018; Accepted 29 November 2018
Available online 30 November 2018
0041-624X/

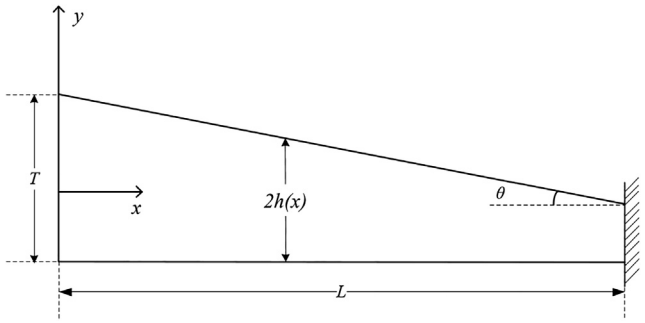

Fig. 1. The schematic of the plate with a linearly-varying thickness.

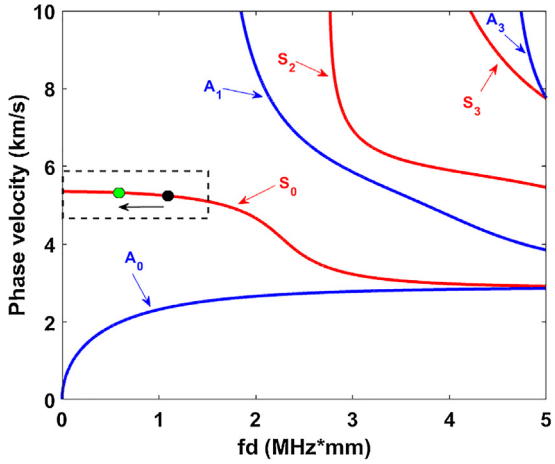

Fig. 2. Phase velocity dispersion curves of Lamb modes in aluminum plates with respect to the *fd*. Symmetric modes are marked red, and asymmetric modes are marked blue. The box region indicates the low frequency region of the S_0 mode.

velocity dispersion curve towards the green dot. With the decreases of *fd*, the difference between phase velocities of the primary wave $c_p(\omega)$ and the harmonic wave $c_p(2\omega)$ becomes smaller as shown in Fig. 2. And, the derivation from the exact phase velocity matching, which is defined as $k_d = 2\omega/c_p(2\omega) - 2\omega/c_p(\omega)$, will also become smaller when the *fd* value decreases. The dispersion length$L$, which is expressed as $L = 2\pi/|k_d|$, will grow larger. As a result, the modal amplitude of the second harmonic wave can still be guaranteed to have a cumulative effect to characterize the material nonlinearity.

To meet the requirements for nondestructive testing in practical applications, the displacement of the Lamb wave at the plate surface is convenient to detect. The normal u_y and tangential u_x components of the theoretical displacements of the chosen S_0 Lamb on the plate surface versus *fd* is calculated and shown in Fig. 3. As the *fd* value increases, the theoretical normal-displacement u_{y0} increases as well, but the tangential displacement u_{x0} decreases. Here the subscript "$_0$" represents S_0 mode.

Based on the analyses of the second harmonic wave in an isotropic elastic uniform-thickness plate, a theoretical analysis has been carried out for a plate with a slowly linearly-varying thickness, and the plate is considered to support adiabatic propagating modes. Here, the variable-thickness plate with length L is divided into M segments in the direction of wave propagation, and each single element is measured to be $l = L/M$. And the m^{th} segment x_m is linked to the first one with the relation $x_m = x_1 + (m-1) * l$, where $m = 1,2,\ldots,M$ is the position index. This nonlinear wave-propagation can be solved using the perturbation theory, and the displacement field $\mathbf{u}_0$ induced by the S_0 mode is expressed as [28]

$$\mathbf{u}_0(x_m, y, t) = \mathbf{u}_0^{(1)}(x_m, y, t) + \mathbf{u}_0^{(2)}(x_m, y, t), \tag{1}$$

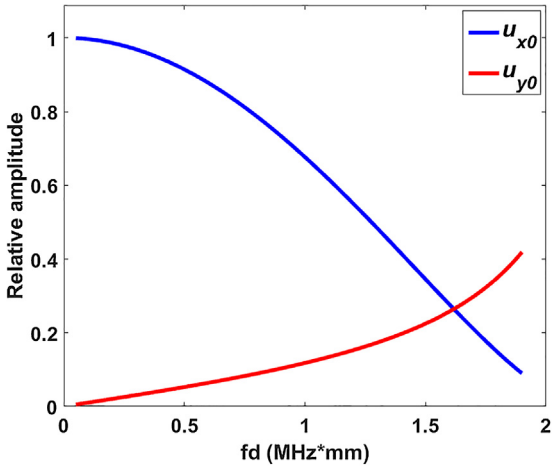

Fig. 3. The displacement components in the × and *y* directions on the surface of plate vs. *fd*.

where $\mathbf{u}_0^{(1)}$ is the primary displacement field, and $\mathbf{u}_0^{(2)}$ is the secondary displacement field, which is very small compared with $\mathbf{u}_0^{(1)}$. Different from the wavenumber expression of a plane wave in a uniform-thickness plate which is presented in Ref. [3]. That is, the wavenumber varies depending on local thickness to form modes along the S_0 mode branch, so that the phase term should be the accumulation of product of the varying wavenumber and the corresponding local segment. In a variable-thickness plate, the appropriate solution for the primary wave field at the m^{th} segment can be written in the form

$$\mathbf{u}_0^{(1)}(x_m, y, t) = \alpha_m \mathbf{U}_0^{(1)}(x_1, y) e^{i[k(x_m)x_m - \omega t]}, \tag{2}$$

where $k(x_m)$ is the local wavenumber of the primary wave at x_m. $\omega = 2\pi f$ is the circular frequency of the chosen mode and f is the frequency. Because the propagation of an adiabatic mode has no reflection and mode conversion, the energy flux of an incident wave remains in S_0 mode propagating along the waveguide and totally passes through the interfaces between neighboring segments. $\mathbf{U}_0^{(1)}(x_1, y)$ is the displacement field vector in the cross section corresponding to the mode at the first segment, which is related to displacement field vector at the m^{th} segment through the proportionality factor α_m. Under the same incident energy flux, the proportionality factor α_m is determined by the ratio of mode energy of the m-th segment $\varphi(x_m)$ to the incident wave energy ϕ_{inc} at the first segment:

$$\alpha_m = \sqrt{\varphi(x_m)/\phi_{inc}}. \tag{3}$$

In the expression, $\varphi(x_m)$ is defined as the poynting vector flow in the propagation direction across the section of a plane elastic plate [29,30]. While, at the second order approximation we have

$$(\lambda + 2\mu)\nabla(\nabla\cdot\mathbf{u}^{(2)}) - \mu\nabla\times(\nabla\times\mathbf{u}^{(2)}) - \rho_0\frac{\partial^2\mathbf{u}^{(2)}}{\partial t^2} = -\mathbf{f}^{(1)}, \tag{4}$$

$$\mathbf{s}_L(\mathbf{u}^{(2)})\cdot\mathbf{n}_r = -\bar{\mathbf{s}}^{(1)}\cdot\mathbf{n}_r, \tag{5}$$

where $\mathbf{s}_L(\mathbf{u}^{(2)})$ is the second order approximation of the first Piola-Kirchhoff stress tensor, and where $\bar{\mathbf{f}}^{(1)}$ and $\bar{\mathbf{s}}^{(1)}$ are the function of $\mathbf{u}_0^{(1)}$. Once the solution $\mathbf{u}_0^{(1)}$ is known, the nonlinear terms $\bar{\mathbf{f}}^{(1)}$ and $\bar{\mathbf{s}}^{(1)}$ are determined by submitting into the equations as following

$$\begin{aligned}\bar{f}_i = &\left(\mu + \tfrac{A}{4}\right)(u_{l,kk}u_{l,i} + u_{l,kk}u_{i,l} + 2u_{i,lk}u_{l,k}) + \left(\lambda + \mu + \tfrac{A}{4} + B\right)\\ &\times(u_{l,ik}u_{l,k} + u_{k,lk}u_{i,l}) + (\lambda + B)(u_{i,kk}u_{l,l}) + \left(\tfrac{A}{4} + B\right)\\ &\times(u_{k,lk}u_{l,i} + u_{k,ik}u_{k,l}) + (B + 2C)(u_{k,ik}u_{l,l}) + O(u_i^3),\end{aligned} \tag{6}$$

$$\bar{s}_{ij} = \left(\frac{\lambda}{2}u_{k,l}u_{k,l} + Cu_{k,k}u_{l,l}\right)\delta_{ij} + Bu_{k,k}u_{j,i} + \frac{A}{4}u_{j,k}u_{k,i} + \frac{B}{2}(u_{k,l}u_{k,l} + u_{k,l}u_{l,k})\delta_{ij} + (\lambda + B)u_{k,k}u_{i,j} + \left(\mu + \frac{A}{4}\right)(u_{i,k}u_{j,k} + u_{k,i}u_{k,j} + u_{i,k}u_{k,j}) + O(u_i^3). \quad (7)$$

where δ_{ij} is the Kronecker delta, $O(u_i^3)$ is the higher order term. Due to zero power flux of SH_0 and A_0 modes from the primary to the second harmonic wave, only S_0 mode is considered in the following analysis [7]. The solution for the second wave field at x_m is expressed in the following equation [3,24]

$$\mathbf{v}^{(2)}(x_m, y, t) = \frac{1}{2}A_0(x_m)\mathbf{v}_0^{(2)}(x_m, y)e^{-i2\omega t} + c.\,c.\,, \quad (8)$$

$$\mathbf{v}^{(2)} = \partial\mathbf{u}^{(2)}/\partial t, \quad (9)$$

where $c.\,c.$ represents the complex conjugate. $\mathbf{v}_0^{(2)}(x_m, y)$ is the particle velocity of 2ω. Furthermore, the modal amplitude $A_0(x_m)$ is the solution of the following ordinary differential equation

$$4P_{00}(x_m)\left(\frac{d}{dx} - ik^*(x_m)\right)A_0(x_m) = (f_0^{surf}(x_m) + f_0^{vol}(x_m))e^{i\int 2k(x_m)dx}, \quad (10)$$

where $k^*(x_m)$ is the local wavenumber of harmonic wave at x_m. As shown in literature [3], due to the self-interaction of the single excited mode, the phase term should be twice the local wave number $k(x_m)$ to satisfy the second harmonic wave excitation condition. Besides, the phase term is accumulating with propagating distance, so the phase term should be the integral of $2k(x_m)$. P_{00} is the complex power flux of S_0 mode in the x-direction of the wave propagation, which can be expressed as

$$P_{00}(x_m) = -\frac{1}{4}\int_{-h(x_m)}^{h(x_m)}\left(\frac{\mathbf{v}_0^*(x_m)}{2}\cdot\frac{\mathbf{s}_0(x_m)}{2} + \frac{\mathbf{v}_0(x_m)}{2}\cdot\frac{\mathbf{s}_0^*(x_m)}{2}\right)\cdot\mathbf{n}_x d\Omega, \quad (11)$$

$\mathbf{s}_0(x_m)$ is the first Piola-Kirchhoff stress tensor, while, f_0^{vol} and f_0^{surf} are interpreted as the power flux through the volume and through the surface, respectively, which can be further expressed as

$$f_0^{surf}(x_m) = -\frac{1}{2}\mathbf{v}_0^*(x_m)\tilde{\mathbf{s}}^{\pm}(x_m)\cdot\mathbf{n}_y\Big|_{y=-h(x_m)}^{y=h(x_m)},$$
$$f_0^{vol}(x_m) = -\frac{1}{2}\int_{-h(x_m)}^{h(x_m)}\tilde{\mathbf{f}}^{\pm}(x_m)\cdot\mathbf{v}_0^*(x_m)dy. \quad (12)$$

From the source condition, we have at the second order the following initial condition for the modal amplitude $A_0(0) = 0$. Hence, Eq. (10) has the solution

$$A_0(x_m) = \bar{A}_0(x_m)e^{i\theta(x_m)} - \bar{A}_0(0)e^{i\theta^*(x_m)}, \quad (13)$$

$$\theta(x_m) = \sum_{m=1}^{m}2k(x_m)l, \quad \theta^*(x_m) = \sum_{m=1}^{m}k^*(x_m)l, \quad (14)$$

where

$$\bar{A}_0(x_m) = i\frac{(f_0^{vol}(x_m) + f_0^{surf}(x_m))}{4P_{00}(x_m)(k^*(x_m) - 2k(x_m))}, \quad (15)$$

$\theta(x_m)$ and $\theta^*(x_m)$ are the cumulative phase term of primary and harmonic wave over the propagated distance respectively, which is the accumulation of product of wavenumber and the corresponding local segment. The phase terms ($k^*(x_m)$, $k(x_m)$) and the energy flux terms of the variable-thickness plates are varying with the propagation distance. And those characteristics have been fully expressed and embodied in Eqs. (13)–(15). Similar to expressions in uniform-thickness plate, the forcing terms $\tilde{\mathbf{f}}^{(1)}$ and $\tilde{\mathbf{s}}^{(1)}$ have a quadratic term of $\mathbf{u}_0^{(1)}$ [28]. And, the second wave field $\mathbf{v}^{(2)}(x_m, y)$ is proportional to the $\tilde{\mathbf{f}}^{(1)}$ and $\tilde{\mathbf{s}}^{(1)}$. So the second harmonic amplitude is proportional to the square of the primary wave amplitude.

The above theoretical method has been developed to investigate the propagation of guided waves along varying thickness plates. And firstly, we studied the influence of frequency of primary wave on second harmonic wave for the plates with same slope by applying the method. A linearly varying thickness aluminum (Al-7075-T651) plate linearly varying from 4 mm to 2 mm (the slope is 0.115°), was considered in this study and the material properties are listed in Table 1. The modal amplitude of second harmonic wave (A_2) with respect to the propagation distance was calculated according to Eqs. (4)–(10) with S_0 mode being the primary mode at fundamental frequencies of 100 kHz, 150 kHz, 200 kHz, and 250 kHz. The propagation distance is set to be 1000 mm and the results are presented in Fig. 4(a–d). It should be noted that, through a lot of calculations and verifications, we have found that the calculated theoretical predictions will be accurate if the smallest wavelength is above10 times more than the length of a single segment. To ensure the adequate accuracy, M (the total amount of the segments) is set to be 2000 in the following calculations, which means that the smallest wavelength is 12.5 times more than the length of a single segment. The magnitudes of the primary wave in the x-and z-directions at $x = 0$, are $u_{0x}^{(1)} = 2.0 \times 10^{-6}$m and $u_{0z}^{(1)} = 2.0 \times 10^{-6}$m, respectively.

Table 1
Material parameters used in numerical simulations [20].

ρ (kg/m^3)	κ (GPa)	μ (GPa)	A (GPa)	B (GPa)	C (GPa)
2810	70.3	26.96	−351.2	−149.4	−102.8

For the primary frequencies of 100 kHz and 150 kHz, the modal amplitude increases monotonically but not linearly within 1000 mm propagating distance. With the frequency being up to 200 kHz, the modal amplitude shows an oscillation at 370 mm, then grows monotonically in the next 630 mm. At 250 kHz, the modal amplitude oscillates spatially almost for four cycles in 700 mm and its spatial periodicity increases as the plate thickness decreases. After the fluctuating range, the modal amplitude increases continually in the remaining distance. Different from the second harmonic wave in a uniform thickness plate, the modal amplitude (A_2) in the varying-thickness plate has slight-dispersion length as presented and defined in Ref. [7].

Besides, aluminum plates linearly varying from 4 mm to 2 mm but with different slopes at a fixed primary frequency were studied. The modal amplitudes of the primary wave (A_1), the second harmonic wave (A_2) and the corresponding relative nonlinearity parameter (A_2/A_1^2) of y-direction displacement u_y were obtained and shown in Fig. 5(a) and (b), respectively. And they-direction displacement at the surface of the plate is convenient to detect by a single beam laser vibrometer in experiments. For the amplitudes of the primary mode (A_1) is changing with the propagating distance, the accumulation of relative nonlinearity parameter (A_2/A_1^2) is not precisely consistent with A_2.

The frequency of the primary wave is 150 kHz, and the slopes of the plates with thickness linearly varying are 0.072°, 0.082°, 0.095°, 0.114°, 0.143°, and 0.191°, respectively. The slope of the plate has certain influences on the generation of the second harmonic wave. As shown in Fig. 5, although the slope of the plate is varying, both the modal amplitudes of second harmonic wave(A_2) and the relative nonlinearity parameter (A_2/A_1^2) increase almost linearly up to 200 mm along the propagation distance. When the slope of the plate is 0.191°, the relative nonlinearity parameter grow almost linearly on the first 500 mm as shown in Fig. 5(b). According to the slopes of the curves shown in the figures, we can validate its cumulative effect. In fact, the larger the slope, the stronger the cumulative effect [20]. For the parameter A_2/A_1^2, as the slope of curve shown in Fig. 5(b), the cumulative effect of plates with a large slope is stronger than that of a small slope. But for the second harmonic wave A_2 shown in Fig. 5(a), the cumulative effect of plates with larger slope is slightly weaker within the distance of 400 mm.

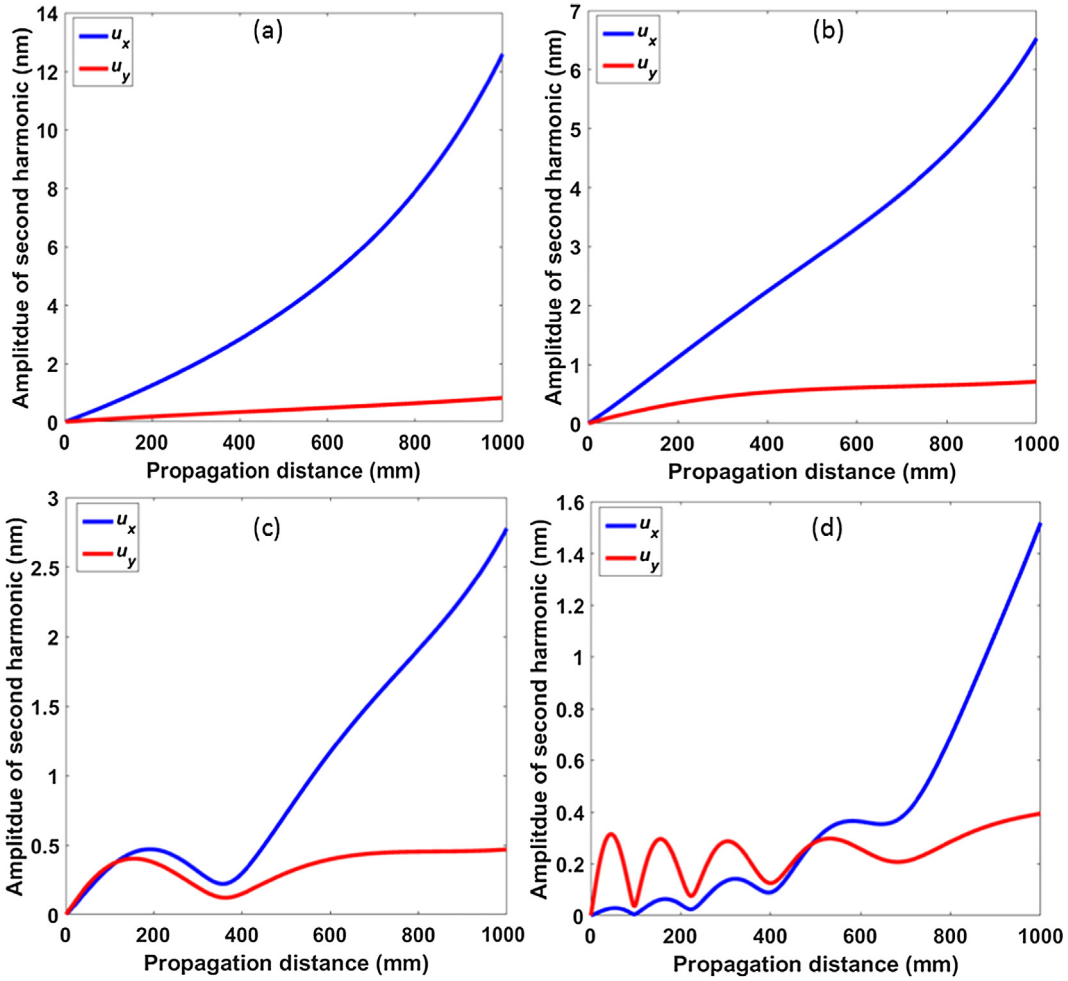

Fig. 4. Variations of second harmonic wave (normalized amplitude) vs. propagation distance for plate with linearly varying thickness, ranging from 4 mm to 2 mm with a slope of 0.115° and at a primary frequency of 100 kHz (a), 150 kHz (b), 200 kHz (c) and 250 kHz (d), respectively.

3. Numerical results

Numerical simulations were carried out to validate the theoretical predictions, which can provide a convenient way to investigate the cumulative harmonic from S_0 mode generation in waveguides and eliminate the nonlinear effects arising out of the physical operations and instrumentations. The numerical simulations were carried out by using the software COMSOL. The Murnaghan model was adopted and plane strain condition was used. The schematic of the varying thickness plate used in simulations is shown in Fig. 1, where the aluminum plate linearly varies from 4 mm to 2.5 mm with a slope of 0.173°. And material properties are listed in Table 1. The source is specified as a displacement boundary condition at × = 0 to excite the appropriate mode, using a 20-cycle Hanning windowed tone-burst with a central frequency of 150 kHz or 250 kHz, respectively. The absorption boundary condition was loaded at the end of the plate and stress free

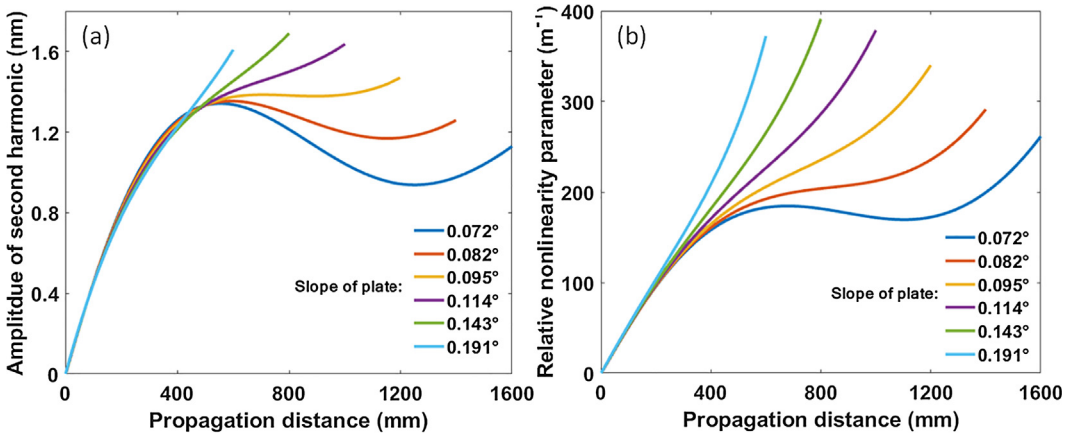

Fig. 5. Modal amplitudes of propagating second harmonic wave (a) and the relative nonlinearity parameter (b) of y-direction displacement u_y for plates with linear thickness variation from 4 mm to 2 mm with different slopes, at a primary frequency of 150 kHz.

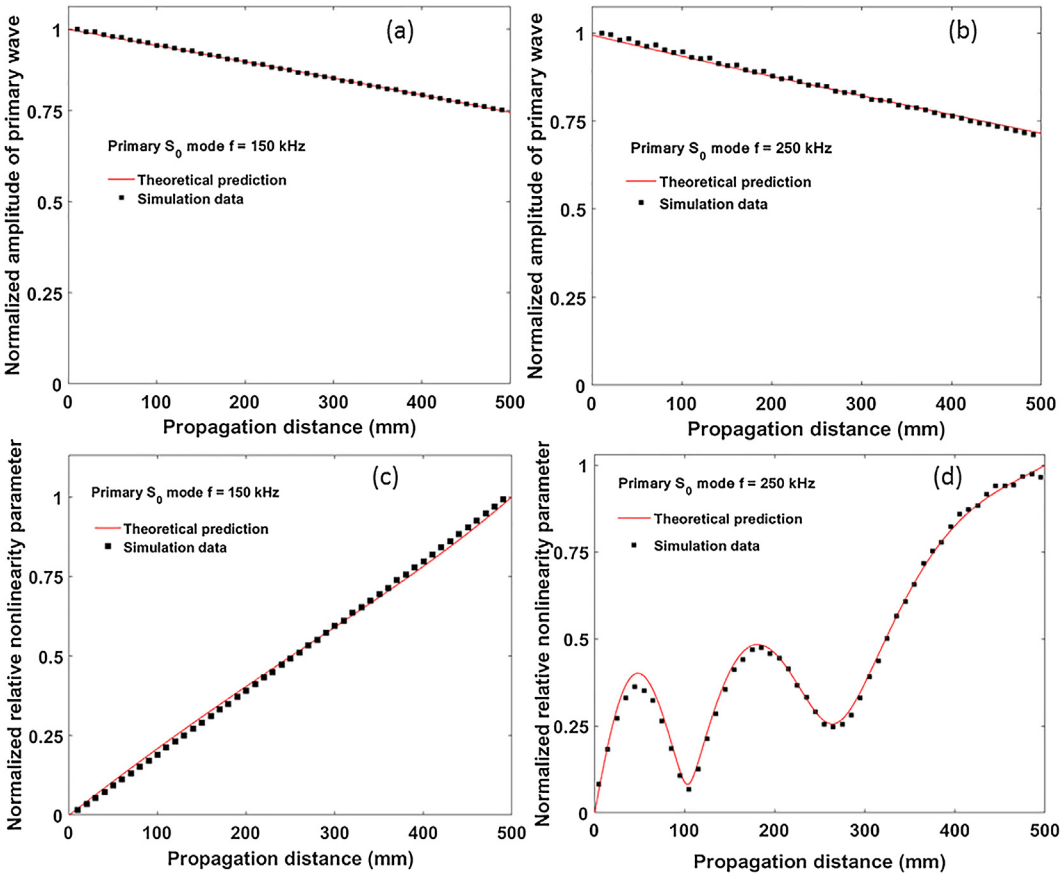

Fig. 6. The normalized amplitude of primary A_1(a-b) and corresponding relative nonlinearity parameter A_2/A_1^2(c-d) of y-direction displacement u_y on the plate surface varying versus propagation distance for plate of linear variation thickness with slope of 0.173°, at a primary frequency of 150 kHz (a and c) and 250 kHz (b and d).

boundary conditions were applied to the rest of the boundaries.

Triangular elements were used. To ensure convergence for both primary and second harmonic modes, the maximum element length is 0.3 mm, and the maximum time step is 0.005 μs. In addition, the monitor points were placed at the lower boundary of the plate to pick up the signal of y-direction displacements in the time domain at a step of 10 mm. The Fast Fourier Transform (FFT) technique was used in post-processing to extract the amplitudes of the primary wave (A_1) and the second harmonic wave (A_2). The amplitudes of the primary wave (A_1) and the calculated relative nonlinearity parameter (A_2/A_1^2) versus propagation distance are shown in Fig. 6. It can be observed that the numerical results agree well with the theoretical predictions. As shown in Fig. 6(a) and (b), with the propagation distance increasing, the amplitude of the primary wave steadily decreases, because the amplitude of the y-direction displacement u_y on the plate surface decreases as corresponding fd decreases as presented in Fig. 3. With the excited frequency of primary S_0 mode at 150 kHz, Fig. 6(c) demonstrates that the relative nonlinearity parameter increases almost linearly up to at least 500 mm. Such a distance is significant for NDT applications of nonlinear Lamb waves in thickness linear variation plate. In Fig. 6(d), when the excitation frequency is 250 kHz, the modal amplitude oscillates almost for two cycles in 280 mm, and then its spatial periodicity gets larger with the propagation distance increasing.

4. Experimental studies

Fig. 7 illustrates the experimental setup to verify the nonlinear features of the S_0 mode on an aluminum varying thickness plate (Al 7075). The material properties of the plate are the same to those listed in Table 1. The excitations were achieved by two wedge transducers in contact, at central frequency of 150 kHz and 250 kHz respectively, coupled to the surface of the plate at $\times = 0$. A 20-cycle Hanning windowed tone-burst signal was generated by a signal generator (Tektronix AFG 3102) and was magnified by a high power gated amplifier. The ultrasonic waves were measured using a laser vibrometer (Polytec PSV-400) to pick up the time-domain signals of the y-direction displacement on the plate surface. The time trace of the signal with 512 averages was recorded by an oscilloscope to improve the signal-to-noise ratio and then processed by a computer. In the experiment, the displacement was measured in the far field along the propagation distance, from 100 to 460 mm with a step of 30 mm. Each set of measurements was repeated independently for seven times. Fig. 8(a and b) show the variation of the amplitude of the primary wave with respect to the propagation distance, while Fig. 8(c and d) show the normalized relative nonlinearity parameters in the distance of propagation with excitation frequency of 150 kHz and 250 kHz, respectively.

Regarding the amplitude of primary wave versus the propagation distance, the experimental results of excitation frequency at 150 kHz and 250 kHz are almost consistent with the theoretical predictions, as shown in Fig. 8(a and b). In the first case, when the excitation frequency is 150 kHz, the linear increase of the relative nonlinearity parameter with the propagation distance is clearly shown from 100 to 460 mm in Fig. 8(c), which demonstrates a cumulative second harmonic generation in this region. When the excitation frequency is 250 kHz, almost one and a half cycles of oscillation is shown in Fig. 8(d) from 100 mm to 460 mm. It should be noted that the first cycle between 0 and 100 mm is difficult to captured experimentally mainly due to the near field effect. Such results agree well with the predictions of theoretical and the numerical calculations, indicating that the amplitude of the second harmonic wave grows linearly in a certain distance in the varying-thickness

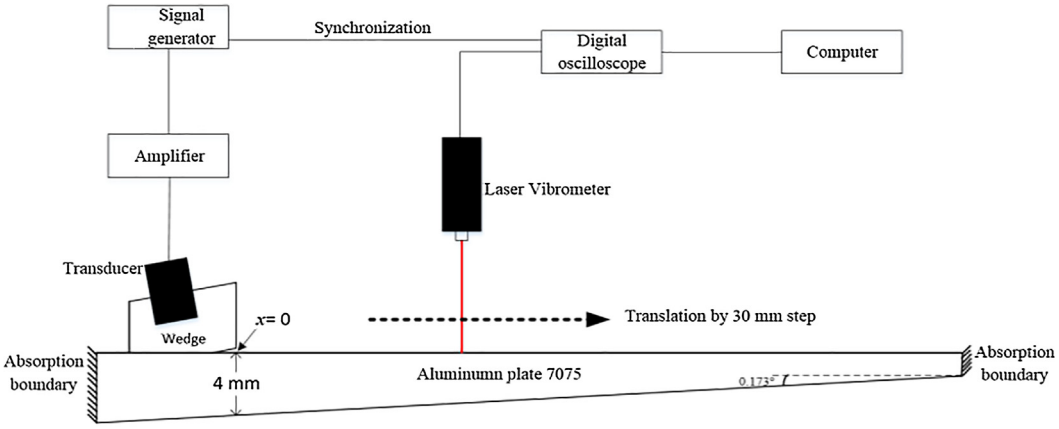

Fig. 7. Experimental setup.

plate in the low frequency range.

The relative nonlinearity parameters of uniform thickness and varying thickness plates are compared at a primary frequency of 250 kHz, as given in Fig. 9. In the uniform-thickness plates, the modal amplitude of the second harmonic wave of u_y remains bounded and oscillates with a constant spatial periodicity. However, for the varying thickness plate, the nonlinear parameter shows a weaker spatial periodicity, its amplitude will not reach zero except at the beginning point, and it is in an upward trend.

5. Conclusions

The second harmonic wave in a varying-thickness plate has been studied, based on the property that the symmetric Lamb mode (S_0) exhibits slight-dispersion in the low *fd* range. A theoretical model of nonlinear guided waves in a slowly linearly-varying-thickness plate has been derived, and it has been verified using numerical simulations and experiments. The cumulative and spatial oscillation properties of low-frequency nonlinear Lamb waves have been discussed. According to the results, the application of nonlinear Lamb wave testing technique may be extended from the uniform-thickness plate to the varying-thickness

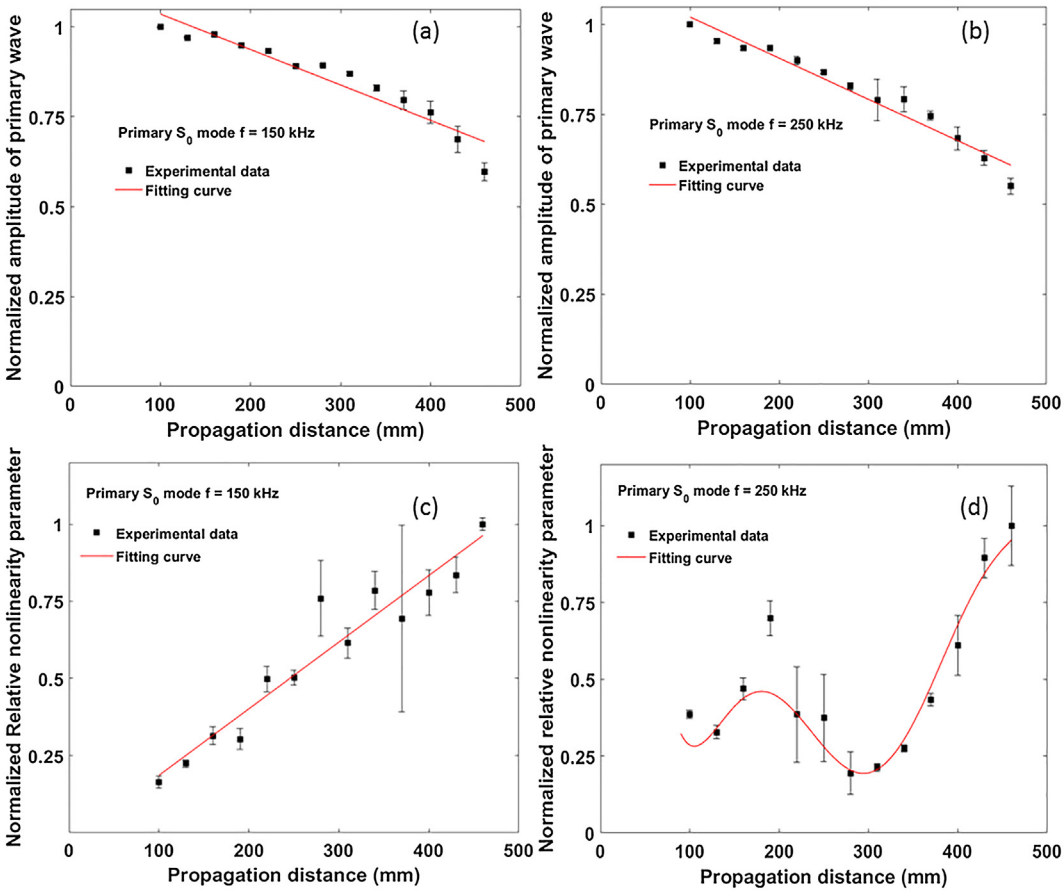

Fig. 8. The normalized amplitude of primary A_1(a-b) and the corresponding relative nonlinearity parameter A_2/A_1^2(c-d) of u_y on the plate surface measured over increasing propagation distance for aluminum plate of thickness linear variation with slope of 0.173°, at excitation frequency of 150 kHz (a and c) and 250 kHz (b and d).

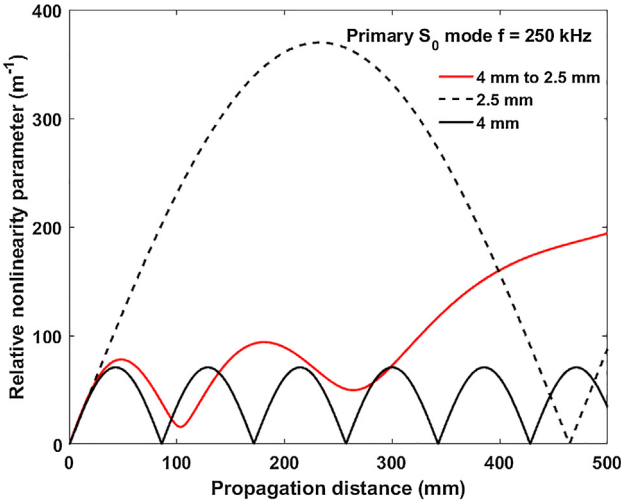

Fig. 9. The relative nonlinearity parameter at the y-direction for the plate with linearly-varying thickness of the slope being 0.173°, and relative nonlinearity parameters of uniform-thickness plates with thickness being 2.5 mm and 4 mm, respectively, at the primary frequency of 250 kHz.

plate.

Acknowledgement

This work was supported by the National Natural Science Foundations of China, under grant Nos. 11427809 and 11874386, and IACAS Young Elite Researcher Project under grant No. QNRC201615. The authors would like to thank Dr. Hanyin Cui from Institute of Acoustics, Chinese Academy of Sciences and Dr. Peng Zuo from Nanyang Technology University for useful discussions.

Appendix A. Supplementary material

Supplementary data to this article can be found online at https://doi.org/10.1016/j.ultras.2018.11.013.

References

[1] M. Deng, Cumulative second-harmonic generation accompanying nonlinear shear horizontal mode propagation in a solid plate, J. Appl. Phys. 84 (1998) 3500–3505.
[2] M. Deng, Cumulative second-harmonic generation of Lamb-mode propagation in a solid plate, J. Appl. Phys. 85 (1999) 3051–3058.
[3] W.J.N. de Lima, M.F. Hamilton, Finite-amplitude waves in isotropic elastic plates, J. Sound Vibrat. 265 (2003) 819–839.
[4] N. Matsuda, S. Biwa, Phase and group velocity matching for cumulative harmonic generation in Lamb waves, J. Appl. Phys. 109 (2011) 094903.
[5] M. Deng, P. Wang, X. Lv, Experimental verification of cumulative growth effect of second harmonics of Lamb wave propagation in an elastic plate, Appl. Phys. Lett. 86 (2005) 124104.
[6] M. Deng, J. Pei, Assessment of accumulated fatigue damage in solid plates using nonlinear Lamb wave approach, Appl. Phys. Lett. 90 (2007) 121902.
[7] P. Zuo, Y. Zhou, Z. Fan, Numerical and experimental investigation of nonlinear ultrasonic Lamb waves at low frequency, Appl. Phys. Lett. 109 (2016) 021902.
[8] S. Fan, J.E. Michaels, J.L. Sang, In situ estimation of applied biaxial loads with Lamb waves, J. Acoust. Soc. Am. 133 (2013) 677–687.
[9] Y. Liu, V.K. Chillara, C.J. Lissenden, On selection of primary modes for generation of strong internally resonant second harmonics in plate, J. Sound Vibrat. 332 (2013) 4517–4528.
[10] M. Deng, Characterization of surface properties of a solid plate using nonlinear Lamb wave approach, Ultrasonics 44 (Suppl 1) (2006) e1157–e1162.
[11] C. Bermes, J.-Y. Kim, J. Qu, L.J. Jacobs, Nonlinear Lamb waves for the detection of material nonlinearity, Mech. Syst. Signal Process. 22 (2008) 638–646.
[12] V. Krishna Chillara, C.J. Lissenden, Interaction of guided wave modes in isotropic weakly nonlinear elastic plates: Higher harmonic generation, J. Appl. Phys. 111 (2012) 124909.
[13] X. Guo, D. Zhang, J. Zhang, Detection of fatigue-induced micro-cracks in a pipe by using time-reversed nonlinear guided waves: a three-dimensional model study, Ultrasonics 52 (2012) 912–919.
[14] N. Rauter, R. Lammering, Impact damage detection in composite structures considering nonlinear lamb wave propagation, Mech. Adv. Mater. Struct. 22 (2014) 44–51.
[15] J. Zhou, L. Xiao, W. Qu, Y. Lu, Nonlinear Lamb wave based DORT method for detection of fatigue cracks, NDT & E Int. 92 (2017) 22–29.
[16] W. Li, Y. Cho, J.D. Achenbach, Detection of thermal fatigue in composites by second harmonic Lamb waves, Smart Mater. Struct. 21 (2012) 085019.
[17] C. Nucera, F. Lanza di Scalea, Nondestructive measurement of neutral temperature in continuous welded rails by nonlinear ultrasonic guided waves, J. Acoust. Soc. Am. 136 (2014) 2561–2574.
[18] C. Nucera, F. Lanza di Scalea, Nonlinear wave propagation in constrained solids subjected to thermal loads, J. Sound Vibrat. 333 (2014) 541–554.
[19] Z. Zhang, D. Liu, M. Deng, D. Ta, W. Wang, Experimental observation of cumulative second-harmonic generation of lamb waves propagating in long bones, Ultrasound Med. Biol. 40 (2014) 1660–1670.
[20] X. Wan, P.W. Tse, G.H. Xu, T.F. Tao, Q. Zhang, Analytical and numerical studies of approximate phase velocity matching based nonlinear S0 mode Lamb waves for the detection of evenly distributed microstructural changes, Smart Mater. Struct. 25 (2016) 045023.
[21] Y. Cho, Estimation of ultrasonic guided wave mode conversion in a plate with thickness variation, IEEE Trans. Ultrasonics Ferroelectr. Freq. Control 47 (2000) 591–603.
[22] P. Marical, M.E. El-Kettani, M.V. Predoi, Guided waves in elastic plates with Gaussian section variation: experimental and numerical results, Ultrasonics 47 (2007) 1–9.
[23] M.E. El-Kettani, A. Guillet, Guided waves in a plate with linearly varying thickness: experimental and numerical results, Ultrasonics 42 (2004) 807–812.
[24] L. Moreau, J.G. Minonzio, M. Talmant, P. Laugier, Measuring the wavenumber of guided modes in waveguides with linearly varying thickness, J. Acoust. Soc. Am. 135 (2014) 2614–2624.
[25] V.B. Galanenko, On coupled modes theory of two-dimensional wave motion in elastic waveguides with slowly varying parameters in curvilinear orthogonal coordinates, J. Acoust. Soc. Am. 103 (1998) 1752–1762.
[26] V. Pagneux, N. Amir, J. Kergomard, A study of wave propagation in varying cross-section waveguides by modal decomposition. Part I. Theory and validation, J. Acoust. Soc. Am. 100 (1996) 2034–2048.
[27] Z.-T. Hu, Z.-W. An, G.-X. Lian, X.-M. Wang, Propagation properties of backward lamb waves in plate investigated by dynamic photoelastic technique, Chinese Phys. Lett. 34 (2017) 114301.
[28] P. Zuo, Y. Zhou, Z. Fan, Numerical studies of nonlinear ultrasonic guided waves in uniform waveguides with arbitrary cross sections, AIP Adv. 6 (2016) 075207.
[29] Z. Hamitouche, M.E.-C. El-Kettani, J.L. Izbicki, H. Djelouah, Reflection at the cut-off and transmission by tunnel effect in a waveguide with linear section variation, Acta Acustica United Acustica 95 (2009) 789–794.
[30] B. Morvan, et al., Lamb wave reflection at the free edge of a plate, J. Acoust. Soc. Am. 113 (2003) 1417–1425.